Clays and Clay Minerals, Vol. 45, No. 2, 194–202, 1997.

THERMAL CHARACTERIZATION OF POLY(STYRENE SULFONATE)/LAYERED DOUBLE HYDROXIDE NANOCOMPOSITES

CHRISTOPHER O. ORIAKHI, ISAAC V. FARR AND MICHAEL M. LERNER

Department of Chemistry and Center for Advanced Materials Research,
Oregon State University, Corvallis, Oregon 97331

Abstract—Phase and morphological changes during thermolysis of $Mg_4Al_2(OH)_{12}CO_3 \cdot nH_2O$ and $Zn_6Al_2(OH)_{16}CO_3 \cdot nH_2O$ layered double hydroxides (LDH) and their nanocomposites with poly(styrene sulfonate) (PSS) are studied by X-ray powder diffraction (XRD), scanning and transmission electron micrography (SEM and TEM) and thermal analyses. $Mg_4Al_2(OH)_{12}CO_3 \cdot nH_2O$ and $Mg_2Al(OH)_6[CH_2CH(C_6H_4SO_3)] \cdot 3H_2O$ show comparable thermal stabilities: the layered structure is lost above 300 °C with the nucleation of the MgO phase at approximately 400 °C and the $MgAl_2O_4$ phase at approximately 800 °C. $Zn_3Al(OH)_8[CH_2CH(C_6H_4SO_3)] \cdot nH_2O$ undergoes complete oxidative pyrolysis of the polyanion by 500 °C. Crystalline oxide products are obtained at a temperature approximately 300 °C lower than that of thermolysis of $Zn_6Al_2(OH)_{16}CO_3 \cdot nH_2O$. The SEM and TEM images show that the thermolysis of LDH carbonates produces dense aggregates containing microcrystalline particles, whereas $Mg_2Al(OH)_6[CH_2CH(C_6H_4SO_3)] \cdot 3H_2O$ forms a macroporous solid.

Key Words—Layered Double Hydroxides, Nanocomposites, Poly(styrene sulfonate).

INTRODUCTION

A need for new solid materials has resulted in the investigation of new synthetic methodologies (Whitesides et al. 1991; Komarneni 1992; Ozin 1992). Increasingly complex specifications of properties have led to the investigation of processes where macro-, micro- and nano-scale structure can be controlled. Layered double hydroxides exhibit properties useful towards many technological applications, including catalysis (Constantino and Pinnavaia 1995; Reichle 1985), ion/proton conduction (DeRoy et al. 1985), anion exchange (Ookubo et al. 1993) and antacid activity (Playle et al. 1974). They may also be envisioned as useful precursors to a wide variety of technological materials.

The LDH structure consists of brucite-like $[M(II)_{1-x}M(III)'_x(OH)_2]^{x+}$ sheets where charge is compensated by anions present within interlayer galleries. Although an LDH prepared in air will incorporate carbonates almost exclusively, a variety of anions can be incorporated into LDH by synthesis under an inert atmosphere. LDH have been prepared with organic anions (Kopka et al. 1988; Chibwe and Jones 1989; Meyn et al. 1990; Park et al. 1990; Carrado et al. 1993; Tagaya et al. 1993; Dutta and Robins 1994; Kuwahara et al. 1994; Raki et al. 1995) and polymeric species (Sugahara et al. 1988; Messersmith and Stupp 1992; Challier and Slade 1994; Oriakhi et al. 1996). With a polymer occupying the 2-dimensional galleries between brucite-like layers, the alternating arrangement of inorganic and organic structures along the stacking direction can be viewed as the nanocomposition of 2 solid phases. Studies of other nanocomposites containing polyethers (Aranda and Ruiz-Hitsky 1992; Lagadic et al. 1992; Wu and Lerner 1993, Lemmon and Lerner 1994; Lemmon and Lerner 1995), conjugated polymers (Ruiz-Hitsky 1993; Oriakhi and Lerner 1995) or structural polymers (Messersmith and Giannelis 1993; Lan and Pinnavaia 1994) indicate that chemical or physical properties such as conductivity, thermal stability and rheology can differ from those of the parent phases or microcomposites. In particular, the thermal properties and thermolysis products of polymer/LDH nanocomposites have been reported to vary according to the molecular weight of the organic component, as well as the nature of interaction between the composited solids (Kuwahara et al. 1994; Messersmith and Stupp 1995). Studies indicate that poly(vinyl alcohol) can be incorporated into the interlayer space of a Ca-Al-LDH (Messersmith and Stupp 1992) and that polymer incorporation results in both an enhanced thermal stability and change in microstructure (Messersmith and Stupp 1995). A poly(acrylonitrile)/LDH nanocomposite has been used as a precursor for the preparation of aluminum nitride ceramics (Sugahara et al. 1988).

We have recently reported on the incorporation of the vinylic polymers, poly(acrylic acid), poly(vinyl sulfonate), and PSS between $M_2Al(OH)_6^+$ (M = Mg, Ca, Co) and $Zn_3M'(OH)_8^+$ (M' = Al, Cr) layers by a templated reaction to form nanocomposites (Oriakhi et al. 1996). The resulting materials contain organic layers with thicknesses of 14.8 to 16.8 Å, which correspond to the incorporation of polymer bilayers between the LDH sheets. In this study, the thermal characteristics and thermolysis products obtained

Table 1. Structural data for LDH carbonates and PSS/LDH nanocomposites.

Sample	c-repeat/ Å	Δd/Å†	domain size/ Å‡
$Mg_4Al_2(OH)_{12}[CO_3]\cdot 3H_2O$	7.63	2.83	890
$Mg_2Al(OH)_6[CH_2CH(C_6H_4SO_3)]\cdot 3H_2O$	20.8	16.0	120
$Zn_6Al_2(OH)_{16}[CO_3]\cdot nH_2O$	7.65	2.85	370
$Zn_3Al(OH)_8[CH_2CH(C_6H_4SO_3)]\cdot nH_2O$	21.6	16.8	110

† Δd = c-repeat − 4.80 Å.

‡ Calculated using the Scherrer relationship of domain size and peak width.

up to 1100 °C from the LDH carbonates $Mg_4Al_2(OH)_{12}CO_3\cdot 3H_2O$ and $Zn_6Al_2(OH)_{16}CO_3\cdot nH_2O$ are contrasted with those of nanocomposites containing PSS.

EXPERIMENTAL

The inorganic starting materials used for all preparations described in this work were analytical reagent grade and used without further purification. Poly(sodium 4-styrene sulfonate), or NaPSS, $M_w \approx 70$ kD was used as obtained from Aldrich Chemical Company. Distilled/deionized water was used in all preparations. $Mg_4Al_2(OH)_{12}CO_3\cdot 3H_2O$, and $Zn_6Al_2(OH)_{16}$-$CO_3\cdot nH_2O$ were prepared from aqueous solutions of the metal nitrates by the precipitation and thermal crystallization method described in Reichle (1985). The gels obtained were aged at 65 °C for 24 h.

LDH-polymer nanocomposites were synthesized by the template method described in Oriakhi et al. (1996), where, using deaerated, aqueous solutions, the polymer and metal salts were simultaneously added to NaOH. Careful deaeration of the solutions and a blanketing inert atmosphere are crucial as the carbonate form preferentially precipitates in the presence of CO_2. In a typical synthesis for the nanocomposite, solutions of $Mg(NO_3)_2\cdot 6H_2O$ (3.16 g, 0.012 mol), $Al(NO_3)_3\cdot 9H_2O$ (2.34 g, 0.0062 mol) and NaOH (3.00 g, 0.075 mol) were added simultaneously to a polymer solution (2.50 g/100 mL) under vigorous stirring. Gels were aged, then filtered, washed several times with hot water to remove excess polymer, and dried *in vacuo* for 24 h. The nanocomposites are air-stable once formed. Samples were heated at temperatures between 25 and 1100 °C in a Thermolyne (type 6000) muffle furnace for 16 h and stored in a desiccator to minimize rehydration.

M(II)/M(III) ratios in the products were taken as the initial mixing ratio, an assumption previously tested in Oriakhi et al. (1996). The water content for the Mg-containing compounds was determined by thermogravimetric analysis (TGA), but not for the Zn-based LDH structures, due to host instability at lower temperatures. Polymer content was determined by elemental analyses for carbon, hydrogen, nitrogen and sulfur (Desert Analytics; Tuscon, Arizona).

The XRD data were collected on a Siemens D5000 powder diffractometer (Cu$K\alpha$ radiation) at 0.02 °2θ sec^{-1} between 2 and 70 °2θ. The XRD sample holders excluded moisture. Products were examined using an AMRAY 1000A scanning electron microscope (SEM) and a Philips CM 12 scanning transmission electron microscope (STEM) at 100 kV. Powder samples for SEM were dusted onto an adhesive dot on 12 mm round glass cover slips on Al mounts, then sputter-coated with approximately 10 nm of 60/40 wt% Au/Pd. Samples for TEM were examined on Cu screens coated with carbon/formvar support film.

Thermal analyses on powder samples (10–20 mg) were carried out using a Shimadzu TGA-50 and DSC-50 in flowing air (50 mL/min) at 10 °C/min. The DSC and derivative TGA data were in close agreement for the samples tested. Surface area measurements were obtained from nitrogen adsorption/desorption isotherms using a Micromeritics ASAP 2000 BET apparatus. Samples were outgassed *in vacuo* overnight at 200 °C prior to BET analyses.

RESULTS AND DISCUSSION

XRD data of the as-prepared materials are summarized in Table 1. The LDH carbonates show longer-range coherence along the stacking direction, as indicated by domain lengths calculated from (00*l*) peak widths. The increased c-repeat distances of the nanocomposites are consistent with the incorporation of a bilayer of PSS between the LDH sheets.

Guest/host ratios are determined from elemental analyses to be $CH_2CH(C_6H_4SO_3)/Mg_2Al(OH)_6 = 1.0$ mol/mol; $CH_2CH(C_6H_4SO_3)/Mg_3Al(OH)_8 = 1.3$; and $CH_2CH(C_6H_4SO_3)/Zn_3Al(OH)_8 = 1.5$. If the mole ratios are normalized for the number of metals in the empirical formulae, there are 1.0, 1.0 and 1.1 mol, respectively, of polymer repeat per 3-metal segment in the LDH structures. The polymer packing in each product is therefore similar, despite the change in sheet charge densities. When the polymer charge exceeds that of the encasing sheets, charge balance might be maintained by the incorporation of sodium ions along with the additional polymer.

$Mg_4Al_2(OH)_{12}CO_3\cdot 3H_2O$, $Mg_2Al(OH)_6[CH_2CH(C_6H_4SO_3)]\cdot 3H_2O$ and Thermolysis Products

The XRD patterns of $Mg_4Al_2(OH)_{12}CO_3\cdot 3H_2O$ and thermolysis products are shown in Figure 1. The layered structure remains well-ordered to about 300 °C. Below 300 °C, the principal change is loss of interparticle and intragallery water (Yun and Pinnavaia 1995), which is reversed by introduction of the sample to moist air. By 400 °C, the materials obtained are mainly amorphous with the first appearance of broad, weak peaks of cubic MgO, and the layer structure is not evident by XRD after heating at 500 °C. The MgO

https://doi.org/10.1346/CCMN.1997.0450207 Published online by Cambridge University Press

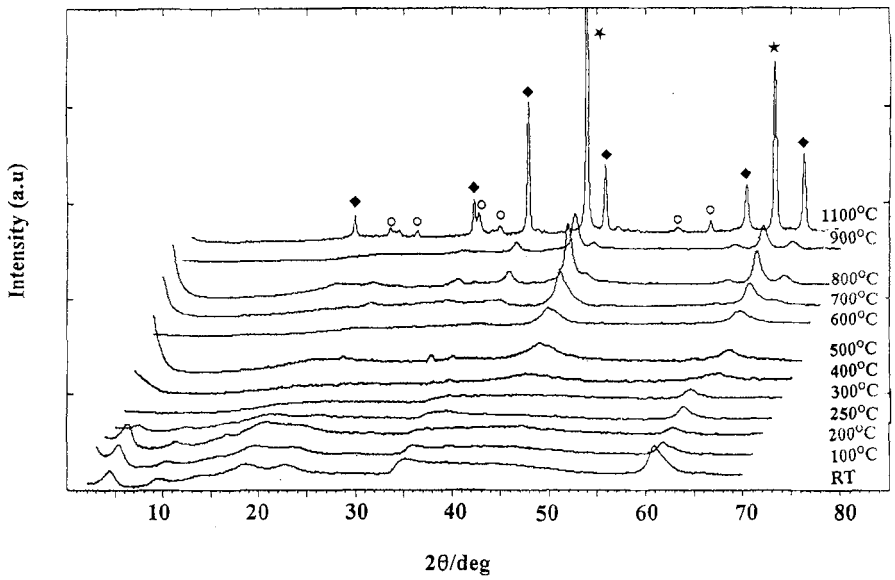

Figure 1. XRD patterns for $Mg_4Al_2(OH)_{12}CO_3{\cdot}3H_2O$ heated at indicated temperatures for 16 h. Peaks are indexed as MgO (★) and $MgAl_2O_4$ (♦).

phase remains poorly crystalline, as evidenced by the 2 broad peaks, until heating at 1100 °C, where the peaks sharpen significantly. An $MgAl_2O_4$ spinel phase first appears in XRD at 900 °C, and produces sharp diffraction peaks after heating at 1100 °C. These observations are consistent with previous observations of the thermolysis of LDH (Cavani et al. 1992) according to:

$$Mg_4Al_2(OH)_{12}CO_3{\cdot}3H_2O\ (s) \rightarrow 3MgO\ (s) + MgAl_2O_4\ (s) + CO_2\ (g) + 9H_2O\ (g) \quad [1]$$

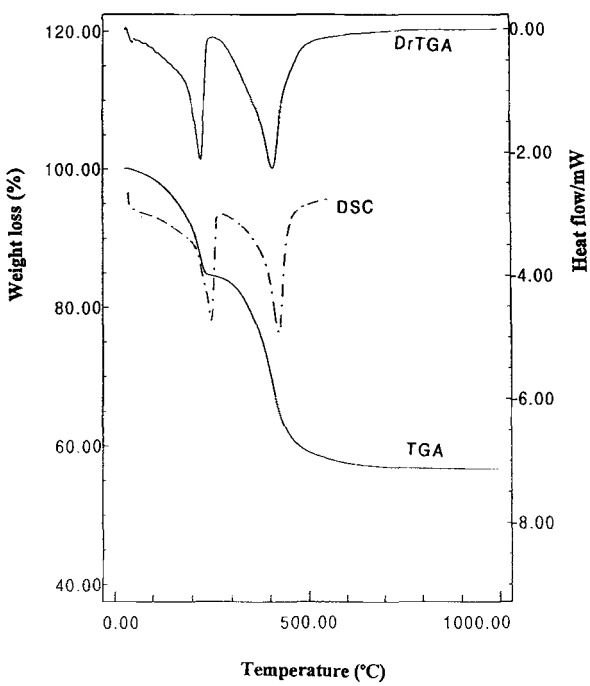

Figure 2. TGA, derivative TGA and DSC traces for $Mg_4Al_2(OH)_{12}CO_3{\cdot}3H_2O$.

Thermal analyses of $Mg_4Al_2(OH)_{12}CO_3{\cdot}3H_2O$ (Figure 2) indicate 2 weight loss endotherms in the temperature range studied; a 15% loss below 210 °C attributed to elimination of surface and intragallery water, and a 28% loss at 300–450 °C from decarboxylation of intersheet CO_3^{2-} and dehydroxylation of the LDH layers (Sato et al. 1986). The total weight loss, 44%, provides a water content of $n = 3$ based on the conversion of the LDH carbonate to oxides according to Equation [1].

The XRD patterns of $Mg_2Al(OH)_6[CH_2CH(C_6H_4SO_3)]{\cdot}3H_2O$ (Figure 3) indicate no irreversible structural changes below 250 °C. The layered nanocomposite peaks begin to disappear after heating above this temperature. The material remains colorless, indicating that the polymer has not carbonized, whereas the material recovered after heating at 400 °C is black. These observations coincide with results of thermal analyses of this compound and Na-PSS (see below), where the onset of polymer degradation occurs at approximately 400 °C. Materials obtained between 400 and 1100 °C show XRD patterns similar to those observed in decomposition products of the carbonate. Several small, unassignable peaks were observed after heating the nanocomposite at 1100 °C.

Three transition regions are observed in thermal analyses of $Mg_2Al(OH)_6[CH_2CH(C_6H_4SO_3)]{\cdot}3H_2O$

https://doi.org/10.1346/CCMN.1997.0450207 Published online by Cambridge University Press

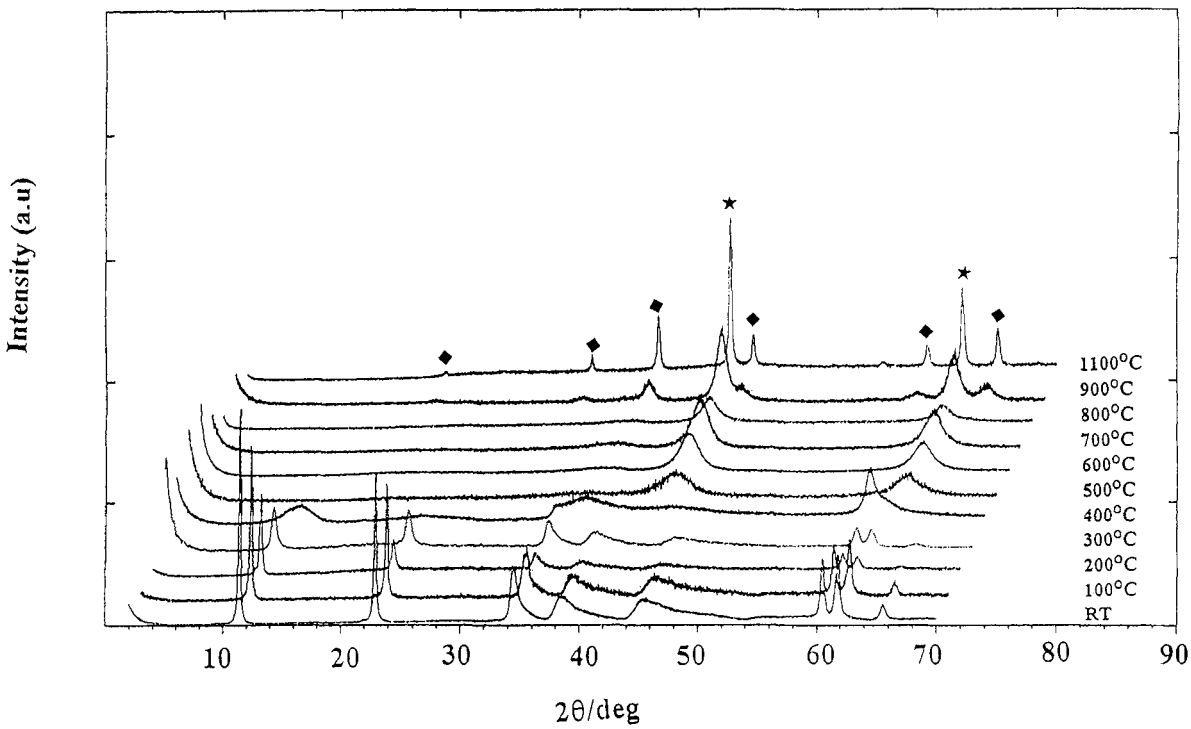

Figure 3. XRD patterns for $Mg_2Al(OH)_6[CH_2CH(C_6H_4SO_3)]\cdot 3H_2O$ heated at indicated temperatures for 16 h. Peaks are indexed as MgO (★), $MgAl_2O_4$ (♦) and unidentified (○).

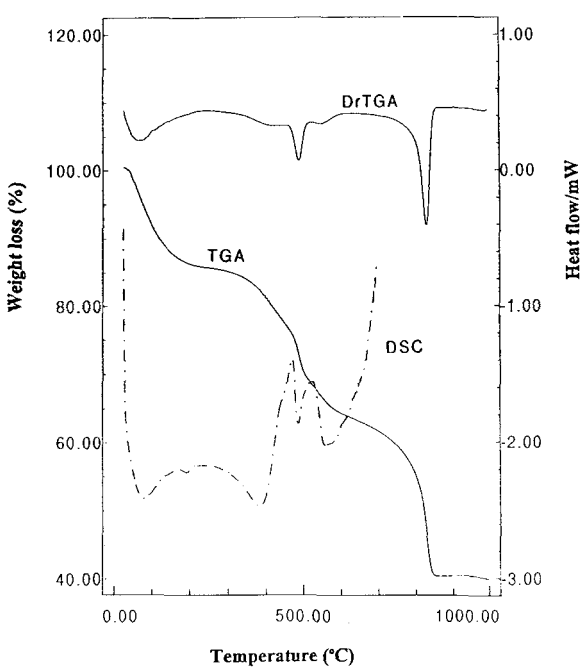

Figure 4. TGA, derivative TGA and DSC traces for $Mg_2Al(OH)_6[CH_2CH(C_6H_4SO_3)]\cdot 3H_2O$.

(Figure 4). First, a 15% loss endotherm, from ambient to approximately 100 °C, is ascribed to the elimination of surface and intragallery water. A 23% loss at 300–500 °C is ascribed to dehydroxylation of the LDH layers and partial decomposition of polymer. The DSC data indicate that this region contains a broad exothermic peak (ascribed to polymer oxidation) and sharper endothermic loss (from LDH dehydration). Finally, a 22% loss at 800 °C is ascribed to the oxidative elimination of the carbonaceous residue generated during initial polymer degradation. The thermal analysis of pure Na-PSS shows a similar high temperature event at 750 °C. Although not described in detail in this report, the nanocomposite prepared with Mg:Al: 3:1 also displays a similar TGA profile.

The mixed oxide recovered after heating the nanocomposite above 900 °C is colorless, indicating the complete elimination of carbon. Based upon the decomposition:

$$Mg_2Al(OH)_6[CH_2CH(C_6H_4SO_3)]\cdot 3H_2O \xrightarrow[-CO_2,CO,SO_2,H_2O]{\Delta} (Mg_2AlO_{3.5}) \quad [2]$$

where $Mg_2AlO_{3.5}$ indicates a stoichiometric mixture of $MgAl_2O_4$ and MgO, the total weight lost obtained by heating to 1100 °C is somewhat less than calculated (calculated 68%, exponential 60%). Several small, un-

https://doi.org/10.1346/CCMN.1997.0450207 Published online by Cambridge University Press

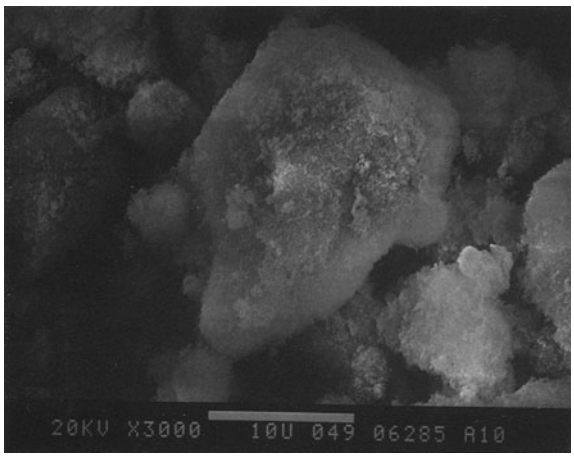

Figure 5. Scanning electron micrograph (SEM) of $Mg_4Al_2(OH)_{12}CO_3{\cdot}3H_2O$ heated at 1100 °C.

identified peaks appear in this product, which may explain this lower weight loss.

In sum, the nanocomposite does not show significantly higher thermal stability than the carbonate form, and produces predominantly the same phases following high-temperature treatment.

The as-prepared $Mg_4Al_2(OH)_{12}CO_3{\cdot}3H_2O$ consists principally of aggregates of submicron crystallites, 0.1 to 0.3 μm in diameter (Oriakhi et al. 1996). After heating to 1100 °C, SEM (Figure 5) shows the formation of denser aggregates with diameters of several μm. Higher magnification reveals that these comprise submicron platelets and needles, approximately similar in microstructure to the material prior to heating.

In contrast, the nanocomposite consists of larger (10 to 100 μm) particles with no observable structural details of submicron dimension (Figure 6a). When heated to 600 °C, the surface microstructure shows evident changes (Figure 6b), and XRD data indicate the presence of cubic MgO in the sample. After heating to 1100 °C (Figure 6c), micrographs show a macroporous structure consisting of fused micron-size particles. The solid contains pores several μm in diameter. BET analyses of the samples (Table 2) indicate relatively low-surface areas, which is reasonable after calcining at these temperatures, so these fused particles are not microporous.

TEM images and area diffraction of the material heated at 1100 °C show that each of the micron-size particles contain multiple crystallites. A higher-resolution image of one particle (Figure 7) shows several crystalline regions. The TEM area diffraction (obtained on a 7-μm diameter spot) matches the bulk sample XRD pattern (Table 3) indicating that both MgO and $MgAl_2O_4$ are represented in each particle.

These data indicate the significant effect of nanocomposition on product macrostructure. The small

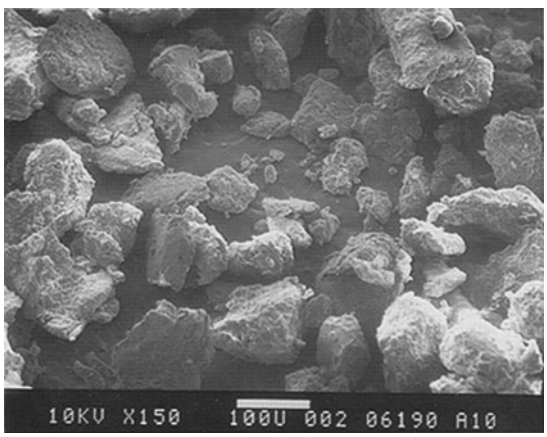

(6a)

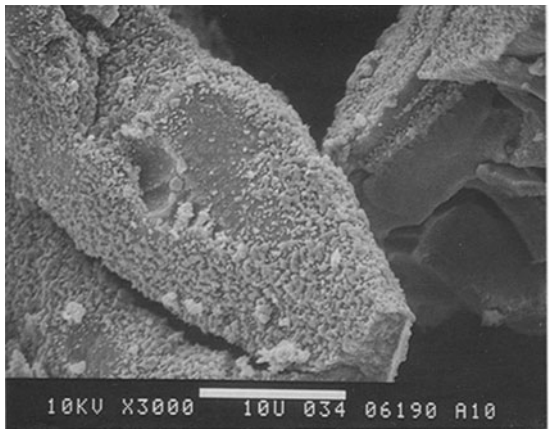

(6b)

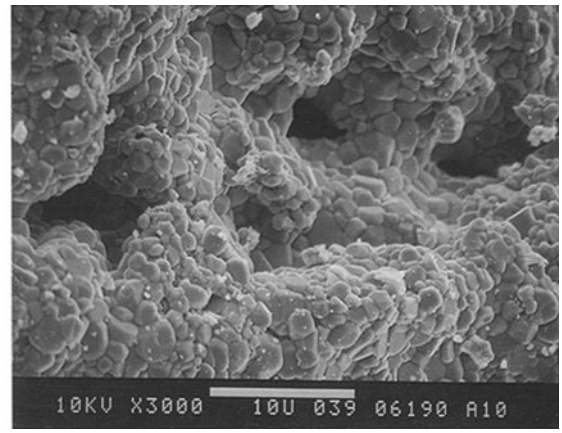

(6c)

Figure 6. SEM of $Mg_2Al(OH)_6[CH_2CH(C_6H_4SO_3)]{\cdot}3H_2O$: a) as prepared; b) heated at 600 °C; and c) heated at 1100 °C.

https://doi.org/10.1346/CCMN.1997.0450207 Published online by Cambridge University Press

Table 2. BET surface areas and average pore diameters for LDH carbonates and PSS/LDH nanocomposites heated at 1100 °C.

Sample	BET surface area m^2/g	Avg pore diameter Å
$Mg_4Al_2(OH)_{12}[CO_3]\cdot 3H_2O$	34.0	158
$Mg_2Al(OH)_6[CH_2CH(C_6H_4SO_3)]\cdot 3H_2O$	2.9	232
$Zn_6Al_2(OH)_{16}[CO_3]\cdot nH_2O$	1.9	142
$Zn_3Al(OH)_8[CH_2CH(C_6H_4SO_3)]\cdot nH_2O$	1.0	92

crystallites obtained by precipitation of the LDH carbonate retain a similar macrostructure after high-temperature treatment. The nanocomposite is precipitated as a less-ordered material with larger particle dimensions and, when heated, forms a macroporous solid. The porosity apparently arises because the loss of organic material occurs in the same temperature range as the nucleation of the final crystalline phases.

$Zn_6Al_2(OH)_{16}CO_3\cdot nH_2O$, $Zn_3Al(OH)_8[CH_2CH(C_6\ H_4SO_3)]\cdot nH_2O$ and Thermolysis Products

The XRD patterns following thermolysis of $Zn_6Al_2(OH)_{16}CO_3\cdot nH_2O$ and $Zn_3Al(OH)_8[CH_2CH(C_6H_4SO_3)]\cdot nH_2O$ provide similar results to those described above: crystalline ZnO and $ZnAl_2O_4$ spinel phases are produced at higher temperatures. (Figures 8 and 9) Both materials become primarily amorphous after heating at 300 °C, but the nanocomposite forms more highly crystalline materials at lower temperatures than the LDH carbonate. The ZnO phase derived from the nanocomposite shows a notable increase in crystallinity from 400 to 500 °C, whereas a similar material is not obtained until the LDH carbonate is heated to 800 °C. Similarly, the spinel phase arises after heating the nanocomposite at 500 °C, but not until heating the carbonate form to 700 to 800 °C.

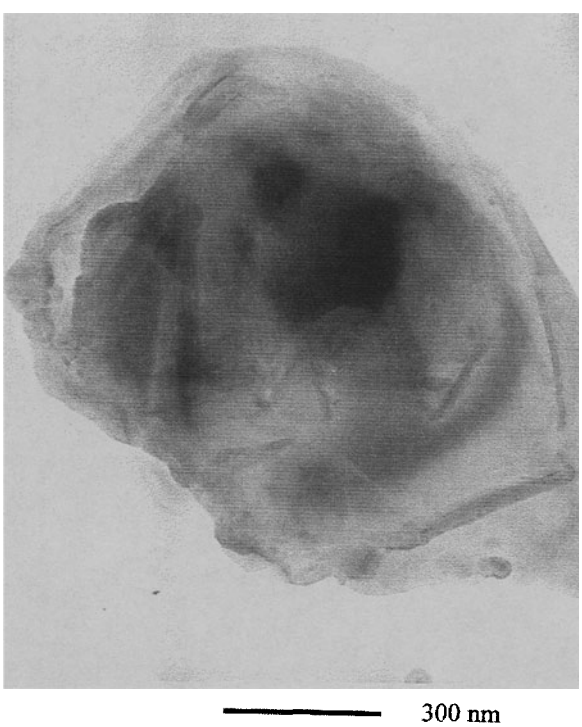

Figure 7. TEM image for $Mg_2Al(OH)_6[CH_2CH(C_6H_4SO_3)]\cdot 3H_2O$ heated at 1100 °C.

Table 3. X-ray and selected area electron diffraction data for $Mg_2Al(OH)_6[CH_2CH(C_6H_4SO_3)]\cdot 3H_2O$ heated at 1100 °C for 16 h.

X-ray diffraction (Å)	Electron diffraction (Å)	Literature values (Å)†	
		MgO (*hkl*)	$MgAl_2O_4$ (*hkl*)
4.667	4.68		4.669 (*111*)
3.929			
3.494			
2.857	2.85		2.859 (*220*)
2.814			
2.640			
2.436	2.42	2.431 (*111*)	2.438 (*311*)
2.333			2.334 (*222*)
2.107	2.13	2.106 (*200*)	
2.020	2.00		2.022 (*400*)
1.649			1.651 (*422*)
1.555	1.56		1.556 (*511, 333*)
1.490	1.49	1.489 (*220*)	
1.429	1.44		1.429 (*440*)
1.366			1.367 (*531*)
	1.23	1.270 (*311*)	1.233 (*533*)
	1.16		1.167 (*444*)
	1.06	1.053 (*400*)	1.053 (*553, 731*)

† Literature data (Galasso 1970) using Fm3m symmetry for MgO with a = 4.2112 Å, Fd3m symmetry for $MgAl_2O_4$ with a = 8.086 Å.

$Zn_6Al_2(OH)_{16}CO_3\cdot nH_2O$ shows a gradual weight loss after the water/CO_2 elimination at 150 to 300 °C (Figure 10). Derivative TGA and especially DSC indicate 2 endotherms in this region, and these may be ascribed to loss of inter- and intra-sheet water, respectively. Thermal analyses for $Zn_3Al(OH)_8[CH_2CH(C_6H_4SO_3)]\cdot nH_2O$ (Figure 11) indicate that PSS decomposes exothermically within the galleries at 450 to 550 °C: the native Na-PSS polymer also shows a large weight loss in this range. A second weight loss is seen at 750 °C for Na-PSS and approximately 800 °C for PSS/MgAl-LDH nanocomposite, but is not observed for $Zn_3Al(OH)_8[CH_2CH(C_6\ H_4SO_3)]\cdot nH_2O$. The sharp weight loss in $Zn_3Al(OH)_8[CH_2CH(C_6\ H_4SO_3)]\cdot nH_2O$ between 300 and 500 °C is also illustrated in TGA of the heat-treated materials (Figure 12).

Why does polymer decomposition occur in a single event for this nancomposite? The presence of metal oxide particles might lower the decomposition temperatures for organic polymers. As a test, 1/1 (w/w) physical mixtures of Na-PSS with ZnO or MgO were

https://doi.org/10.1346/CCMN.1997.0450207 Published online by Cambridge University Press

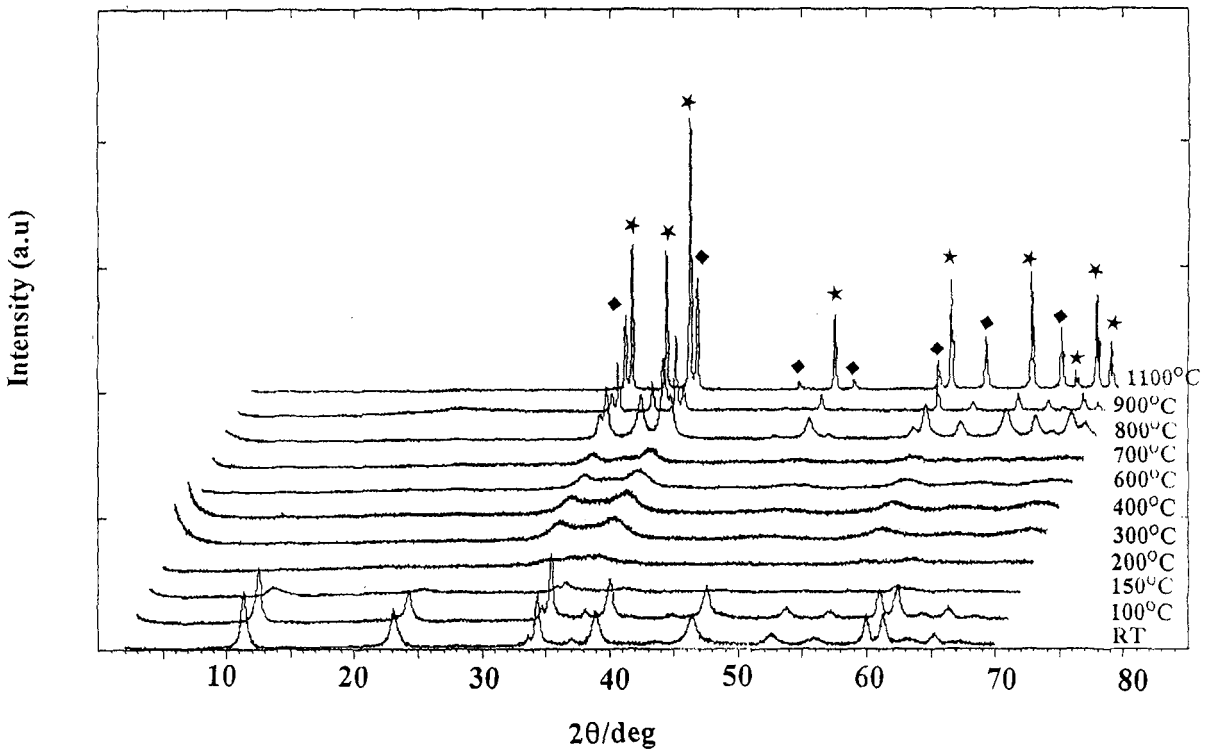

Figure 8. XRD patterns for $Zn_6Al_2(OH)_{16}CO_3{\cdot}nH_2O$ heated at indicated temperatures for 16 h. Peaks are indexed as ZnO (★) and $ZnAl_2O_4$ (◆).

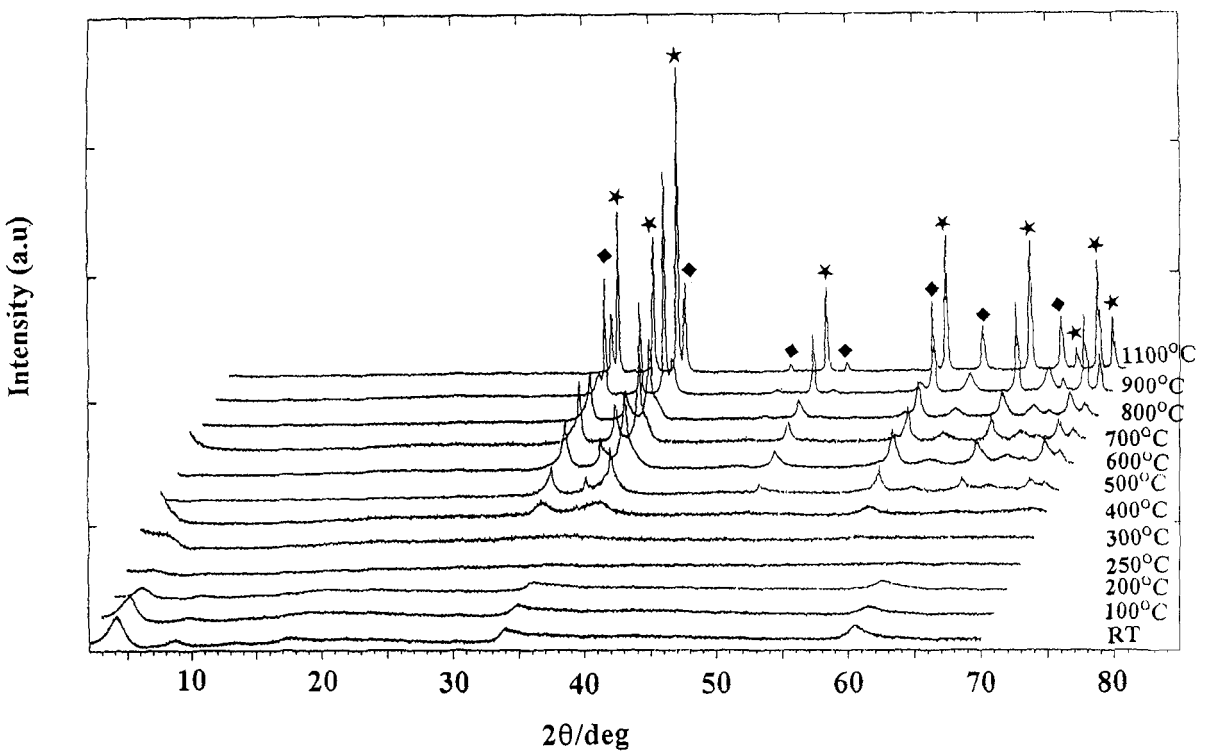

Figure 9. XRD patterns for $Zn_3Al(OH)_8[CH_2CH(C_6H_4SO_3)]{\cdot}nH_2O$ heated at indicated temperatures for 16 h. Peaks are indexed as ZnO (★) and $MgAl_2O_4$ (◆).

https://doi.org/10.1346/CCMN.1997.0450207 Published online by Cambridge University Press

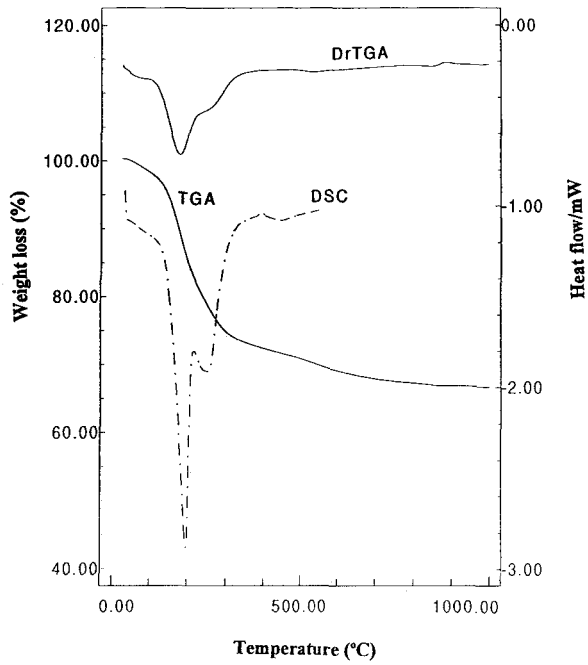

Figure 10. TGA, derivative TGA and DSC traces for $Zn_6Al_2(OH)_{16}CO_3{\cdot}nH_2O$.

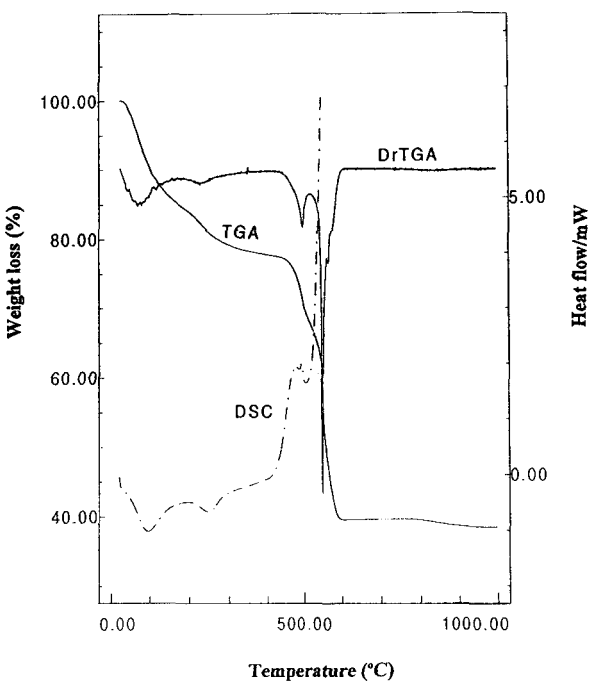

Figure 11. TGA, derivative TGA and DSC traces for $Zn_3Al(OH)_8[CH_2CH(C_6H_4SO_3)]{\cdot}nH_2O$.

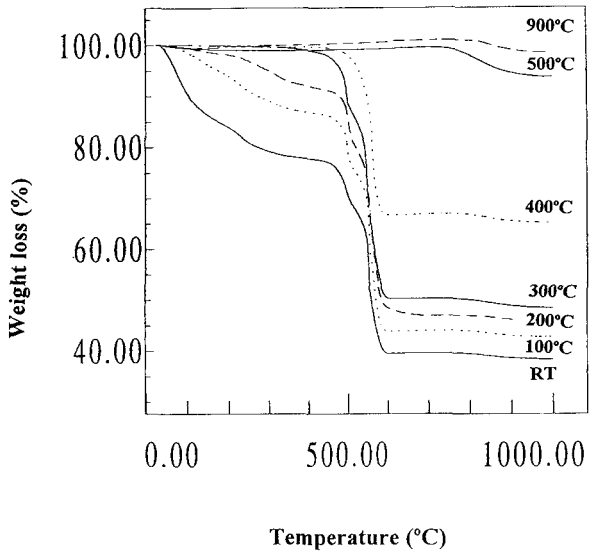

Figure 12. TGA for $Zn_3Al(OH)_8[CH_2CH(C_6H_4SO_3)]{\cdot}nH_2O$ heated at indicated temperature for 16 h.

examined by TGA. In each case, complete polymer degradation was observed in a single event, at 450 to 500 °C for ZnO, and 400 to 600 °C for MgO. Therefore, it is suggested that the earlier appearance of ZnO allows for the lower-temperature loss of the polymer in $Zn_3Al(OH)_8[CH_2CH(C_6H_4SO_3)]{\cdot}nH_2O$.

Alternatively, the thermodynamic stabilities of reactants and products can be considered: the inclusion of p-toluenesulfonate into an MgAl-LDH host is reported to result in an increased thermolysis temperature relative to its sodium salt (Kuwahara et al. 1994). This effect was explained in terms of the thermodynamic stabilities associated with the sodium and nanocomposited forms of the organoanion.

ACKNOWLEDGMENTS

The authors gratefully acknowledge supporting grant DMR-9322071 from the National Science Foundation. We thank G. Rorrer and T.-Y. Hsien in Oregon State University Chemical Engineering for assistance with surface area measurements, and A. Soeldner for help with electron microscopy.

REFERENCES

Aranda P, Ruiz-Hitsky E. 1992. Poly(ethylene oxide)-silicate intercalation materials. Chem Mater 4:1395–1403.

Carrado KA, Forman JE, Botto RE, Winans RE. 1993. Incorporation of phthalocyanines by cationic and anionic clays vis ion exchange and direct synthesis. Chem Mater 5:472–478.

Cavani F, Trifiro F, Vaccari A. 1992. Hydrotalcite-type anionic clays: Preparation, properties and applications. Catal Today 11:173–301.

Challier T, Slade RTC. 1994. Nanocomposite materials: Polyaniline-intercalated layered double hydroxides. J Mater Chem 4:367–371.

Chibwe K, Jones W. 1989. Intercalation of organic and inorganic anions into layered double hydroxides. J Chem Soc, Chem Commun:926–927.

Constantino VRL, Pinnavaia TJ. 1995. Basic properties of $Mg^{2+}_{1-x}Al^{3+}_{x}$ layered double hydroxides intercalated by carbonate, hydroxide, chloride, and sulfate anions. Inorg Chem 34:883–892.

DeRoy A, Besse JP, Bondot P. 1985. Structural approach and conductivity of lamellar hydroxides $Zn_2Cr(OH)_6X{\cdot}nH_2O$ (X = anion) by XANES, EXAFS and X-ray diffraction. Mater Res Bull 20:1091–1098.

Dutta PK, Robins DS. 1994. Pyrene sorption in organic-layered double-metal hydroxides. Langmuir 10:1851–1856.

Galasso FS. 1970. Structure and properties of inorganic solids. Oxford: Pergamon Pr. 297 p.

Komarneni S. 1992. Nanocomposites. J Mater Chem 2: 1219–1230.

Kopka H, Beneke K, Lagaly G. 1988. Anionic surfactants between double metal hydroxide layers. J Colloid Interface Sci 123:427–436.

Kuwahara T, Onitsuka O, Tagaya H, Kadokawa J, Chiba K. 1994. Thermal characterization of the compound of p-toluenesulfonate into a layered double hydroxide. J Incl Phenom Mol Recogn Chem 18:59–68.

Lagadic I, Leastic A, Clement R. 1992. Intercalation of polyethers into MPS_3 (M=Mn, Cd) host lattice. J Chem Soc, Chem Commun:1396–1397.

Lan T, Pinnavaia TJ. 1994. Clay-reinforced epoxy nanocomposites. Chem Mater 6:2216–2219.

Lemmon JP, Lerner MM. 1994. Preparation and characterization of nanocomposites of polyethers and molybdenum disulfide. Chem Mater 6:207–210.

Lemmon JP, Lerner MM. 1995. Preparation of nanocomposites of poly(ethylene oxide) with TiS_2. Solid State Commun 94:533–537.

Messersmith PB, Giannelis EP. 1993. Polymer-layered silicate nanocomposites: *in situ* intercalative polymerization of ϵ-caprolactone in layered silicates. Chem Mater 5:1064–1066.

Messersmith PB, Stupp SI. 1992. Synthesis of nanocomposites: Organoceramics. J Mater Res 7:2599–2611.

Messersmith PB, Stupp SI. 1995. High-temperature chemical and microstructural ransformations of a nanocomposite organoceramic. Chem Mater 7:454–460.

Meyn M, Beneke K, Lagaly G. 1990. Anion-exchange reactions of layered double hydroxides. Inorg Chem 29: 5201–5207.

Ookubo A, Kenta Ooi A, Hayashi H. 1993. Preparation and phosphate ion-exchange properties of a hydrotalcite-like compound. Langmuir 9:1418–1422, and references contained therein.

Oriakhi CO, Farr IV, Lerner MM. 1996. Incorporation of poly(acrylic acid), poly(vinylsulfonate) and poly(styrenesulfonate) within layer double hydroxides. J. Mater Chem 6:103–107.

Oriakhi C, Lerner M. 1995. Poly(pyrrole) and poly(thiophene)/clay nanocomposites via latex colloid interaction. Mater Res Bull 30:723–729.

Ozin GA. 1992. Nanochemistry: Synthesis in diminishing dimensions. Adv Mater 4:612–649.

Park IY, Kuroda K, Kato C. 1990. Direct synthesis of intercalation compounds between a layered double hydroxide and an anionic dye. J Chem Soc Dalton Trans:3071–3074.

Playle AC, Gunning SR, Llewellyn AF. 1974. The in vitro antacid and anti-pepsin activity of hydrotalcite. Pharm Acta Helv 49:298–302.

Raki L, Rancorut DG, Detellier C. 1995. Preparation, characterization, and mossbauer spectroscopy of organic anion intercalated pyroaurite-like layered double hydroxides. Chem Mater 7:221–224.

Reichle WT. 1985. Catalytic reactions by thermally activated, synthetic, anionic clay minerals. J Catal 94:547–557.

Ruiz-Hitsky E. 1993. Conducting polymers intercalated in layered solids. Adv Mater 5:334–340.

Sato T, Wakayoshi T, Shimada M. 1986. Adsorption of various anions by magnesium aluminum oxide ($Mg_{0.7}Al_{0.3}O_{1.15}$). Ind Eng Chem Res 25:89.

Sugahara Y, Yokoyama N, Kuroda K, Kato C. 1988. AIN formation from a hydrotalcite-polyacrylonitrile intercalation compound by carbothermal reduction. Ceram Int 14: 163–167.

Tagaya H, Sato S, Morioka H, Kodakawa J, Karasu M, Chiba K. 1993. Preferential intercalation of isomers of naphthalenecarboxylate ions into the interlayer of layered double hydroxides. Chem Mater 5:1431–1433.

Whitesides GM, Mathias JP, Seto CT. 1991. Molecular self-assembly and nanochemistry: A chemical strategy for the synthesis of nanostructures. Science 254:1312–1319.

Wu J, Lerner MM. 1993. Structural, thermal, and electrical characterization of layered nanocomposites derived from Na-montmorillonite and polyethers. Chem Mater 5:835–838.

Yun SK, Pinnavaia TJ. 1995. Water content and particle texture of synthetic hydrotalcite-like layered double hydroxides. Chem Mater 7:348–354.

(Received 9 February 1996; accepted 29 April 1996; Ms. 2737)